AIMS Energy, 14(1): 23–46.
DOI: 10.3934/energy.2026002
Received: 08 September 2025
Revised: 30 November 2025
Accepted: 19 December 2025
Published: 06 January 2026

https://www.aimspress.com/journal/energy

Research article

Parameter identification and state of charge estimation for lithium-ion batteries based on trust region least squares

Jun Wang[1,2], Dexing Wang[3], Hui Li[2], Chao Ma[2], Changhai Liu[3] and Bin Wang[3,*]

[1] Institute for Advanced Materials and Technology, University of Science and Technology Beijing, Beijing 100083, China
[2] State Key Laboratory of Environmental Adaptability for Industrial Products, China National Electric Apparatus Research Institute Co., Ltd, Guangzhou 510663, China
[3] School of mechanical engineering, Xi'an Jiaotong University, Xi'an 710049, China

* **Correspondence:** Email: b.wang@xjtu.edu.cn; Tel: +8615891448179.

Abstract: To address issues of inaccurate parameter identification and large state of charge (SOC) estimation error for lithium-ion batteries in electric vehicle (EV) applications, we proposed a parameter identification and corresponding SOC estimation method based on a trust region least squares (TRLS) algorithm. First, a second-order resistor-capacitor (RC) equivalent circuit model for the lithium-ion battery was established. To effectively describe the dynamic characteristics of the lithium-ion battery, discharge experiments were designed and conducted to collect the data of terminal voltage, current, and time. The initial parameters of this model were then obtained through a segmented identification based on the Levenberg-Marquardt (LM) algorithm. Subsequently, an improved parameter identification algorithm based on the TRLS was constructed. This algorithm conducted the iterative optimization of model parameters by searching for the best solution within the trust region, thereby achieving precise identification of model parameters. Finally, the SOC estimation was achieved using the TRLS-based optimization solution of model parameters in conjunction with the dual extended Kalman filter (DEKF) algorithm. With the proposed TRLS-based method, the Mean Absolute Error (MAE) values of the estimated SOC were 0.0031, 0.0066, 0.0052, and 0.0044 under the static open-circuit voltage (OCV), the dynamic Urban Dynamometer Driving Schedule (UDDS), Hybrid Pulse Power Characterization (HPPC), and Dynamic Stress Test (DST) conditions, respectively. The comparative results successfully verified the reliability and effectiveness of the proposed TRLS-based method, which demonstrated significant potential and advantages for battery management applications.

Keywords: lithium-ion battery; parameter identification; state of charge estimation; trust region least squares; dual extended kalman filter

1. Introduction

Against the backdrop of the rapid development of new energy technologies, lithium-ion batteries, as efficient energy storage and conversion devices, have become core components in modern transportation systems due to their significant advantages such as high energy or power density, long cycle life, low self-discharge rate, and environmental friendliness [1,2]. Undoubtedly, the high energy density, rapid charging capability, and long cycle life of lithium-ion batteries would significantly enhance the driving range and the travel flexibility of electric vehicles (EVs), while their efficient energy storage characteristics and low self-discharge rate would further reduce energy consumption compared with the conventional internal-combustion engine (ICE) vehicles [3,4]. Moreover, the intelligent integration of state monitoring and power control in a battery management system (BMS) would provide reliable support for the health monitoring, performance optimization, and lifespan extension of EVs, which would reduce the long-term operating cost and show broad application prospects [5,6]. In the future, with the continuous progress of new energy technologies, lithium-ion batteries are expected to be applied in various fields, including renewable energy storage systems, energy storage devices in smart grids, portable power supplies, and so on [7,8].

To achieve efficient energy management for a lithium-ion battery system, it is crucial to establish a model and identify the relevant model parameters for every cell [9,10]. However, the model establishment and the corresponding parameter identification would encounter numerous technical challenges and difficulties in practical applications. Since lithium-ion batteries involve the coupling of nonlinear dynamic operation characteristics in multiple physical fields, it is very difficult to accurately describe them using a simple model [11,12]. Moreover, battery model parameters such as internal resistance and capacity would exhibit nonlinear and time-varying changes along with dynamic factors such as the performance degradation, the charge or discharge rate, and the variable state of charge (SOC) [13,14]. Therefore, it is very necessary to establish a reasonable and reliable model that reflects the dynamic operation characteristics of lithium-ion batteries and identify the corresponding parameters for achieving the precise estimation of the real-time SOC or other states in battery management applications.

Commonly used battery models include the electrochemical models, data-driven models, and equivalent circuit models [15,16]. The electrochemical models are so complex that the identification process might be incomprehensible [17]. The data-driven models need high computational load for the microprocessor, which poses a significant challenge for these compact and integrated battery energy storage systems [18]. For equivalent circuit models, the second-order resistor-capacitor (RC) equivalent circuit considers the approximation of electrochemical processes and the lag characteristic of the lithium-ion battery, which would effectively describe the dynamic response of the output voltage based on different branches of the introduced RC elements during dynamic charge or discharge conditions [19,20]. However, the coupling among parameters in the second-order RC model makes it difficult to achieve separate parameter identification [21]. Furthermore, improper selection of initial values for the identification of model parameters might lead to convergence to a local optimum, which would result in low identification accuracy and significant deviation between the final model-fitted

voltage and the measured result for the lithium-ion battery.

In recent years, accurate identification methods for the second-order RC equivalent circuit parameters of lithium-ion batteries have garnered significant attention in the field of battery management. To achieve the accurate parameter identification for lithium-ion batteries, the least squares methods, Kalman filter or particle filter algorithms, genetic algorithms, or neural network-based techniques have been extensively explored [22]. Among these methods, the least squares methods stand out for their simplicity and computational efficiency. However, its performance is notably compromised in the presence of noise, which might result in significant deviations in parameter estimation, especially under complex conditions with dynamic disturbances [23,24]. To address the noise issue, the extended Kalman filter (EKF), unscented Kalman filter (UKF), and particle filter algorithms have been widely adopted. The EKF relies on the linear approximation, which might reduce the estimation accuracy. In contrast, the UKF conducts the nonlinear evolution of the state distribution through a deterministic sampling strategy, which showed solid performance in several scenarios [25,26], whereas particle filter methods approximate the posterior via Monte-Carlo methods, making them attractive for strongly nonlinear systems [27,28]. Nevertheless, the pursuit of high accuracy with these techniques usually entails a marked increase in computational load. When the state dimension or the particle count grows, the real-time burden on embedded hardware would become pronounced. Consequently, we propose an algorithmic structure that trades off accuracy against efficiency, ensuring suitability for resource-constrained BMS platforms.

In addition to the above-mentioned filter methods, genetic algorithms have gained popularity due to their global search capabilities. This makes them particularly useful in complex optimization problems where traditional methods may struggle [29–31]. Nevertheless, these genetic algorithms are often criticized for their slow convergence speeds and high computational complexity. Apart from the genetic algorithm, the forgetting factor least squares method has shown promise in scenarios where system parameters vary in real-time [32]. However, the corresponding performance or calculation result is highly sensitive to the designed forgetting factor. An inappropriate design of the forgetting factor would lead to the overfitting of recent data under dynamic operating conditions. To improve the identification accuracy under dynamic operation conditions, neural network-based approaches, particularly those based on deep learning, have been extensively studied [33]. Significantly, they require substantial amounts of high-quality labeled data for training, which may not be available in practical applications [34–36]. Since we focus on the joint optimization of model-parameter and state estimation under the real-time constraints of an embedded platform, we use a lightweight architecture that fuses a physics-based model with filtering techniques, ensuring a balance among accuracy, real-time capability, and interpretability [37].

To improve the parameter identification accuracy for lithium-ion batteries based on the equivalent circuit model and accurately reflect their dynamic characteristics, we propose a trust region least squares (TRLS) algorithm integrated with the dual extended Kalman filter (DEKF). The innovation of this study lies in the hybrid approach of the TRLS and the DEKF, which is suitable for the nonlinear dynamic optimization and parameter identification of lithium-ion batteries. Specifically, the TRLS algorithm significantly enhances the initial parameter identification accuracy by constructing a local approximation model within the trust region during the offline phase, effectively addressing the sensitivity to initial guesses of previous methods such as genetic algorithms [38]. This refined initialization process directly improves the robustness of the subsequent online state estimation based on the DEKF method. Compared with the traditional method combining the RLS and EKF algorithms,

the TRLS-based approach provides a more stable and accurate initial point for the DEKF method, mitigating the effects of initial value bias and nonlinearity. Furthermore, by leveraging the precise offline calibration of the TRLS method, the computational burden of the DEKF method during the real-time operation is reduced, alleviating the high computational costs associated with methods such as particle filters. Finally, various comparisons between simulation and experimental test results are conducted under four test conditions, including the static open-circuit voltage (OCV), the dynamic Urban Dynamometer Driving Schedule (UDDS), Hybrid Pulse Power Characterization (HPPC), and Dynamic Stress Test (DST) test conditions. Results would reveal the effectiveness and accuracy of the proposed TRLS-based method for parameter identification and SOC estimation of lithium-ion batteries.

This paper is organized as follows. In Section 2, we establish a second-order RC equivalent circuit model for lithium-ion batteries. In Section 3, we perform the preliminary identification of battery model parameters using the Levenberg-Marquardt (LM) algorithm. In Section 4, we introduce the TRLS-based optimization algorithm to further enhance the accuracy of the parameter identification. In Section 5, we utilize the TRLS-based optimization solution of model parameters and the DEKF algorithm to achieve the accurate SOC estimation. Finally, Conclusions are given in Section 6.

2. Lithium-ion battery model

In battery modeling, equivalent circuit models are widely used for state estimation due to their simplicity, clear physical meaning, and ease of implementation. However, selecting an appropriate model requires a careful trade-off between accuracy and computational complexity, which directly affects its practical application in BMS. The evolution of equivalent circuit models reflects a progression from simplicity to complexity [39]. The basic Rint model, consisting of an ideal voltage source and an ohmic resistor, is simple and easy to parameterize but lacks accuracy due to its inability to describe dynamic polarization. The first-order RC model improves accuracy by introducing a single RC element to simulate electrochemical polarization, but it struggles with complex dynamics. Higher-order RC models enhance accuracy by adding more RC elements to describe multi-time-constant dynamics, but this comes at the cost of increased complexity and computational burden [40,41]. Additionally, advanced models like the Linear Time-Varying Parameter (LTVP) model and Hammerstein model address battery nonlinearity and time-varying characteristics but are often too complex for real-time embedded applications.

As a compromise, the second-order RC model introduces two RC branches to characterize electrochemical and concentration polarization with distinct time constants. This model successfully achieves a balance between accuracy and computational efficiency, making it suitable for practical applications [42,43]. In this paper, the second-order RC equivalent circuit model is established for reflecting the dynamic operation performance of the lithium-ion battery. As shown in Figure 1, in this equivalent circuit model, U_0 represents the OCV, R_0 denotes the ohmic resistance, and R_1 and C_1 represent the electrochemical polarization resistance and capacitance, respectively. Moreover, R_2 and C_2 represent the concentration polarization resistance and capacitance, respectively. U_T represents the actual output voltage, and I represents the operating current.

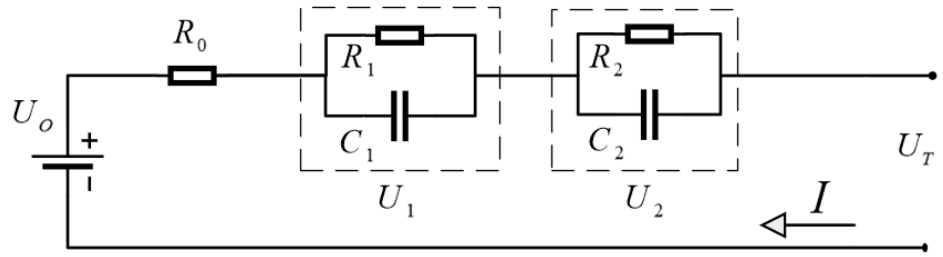

Figure 1. A second-order RC equivalent circuit model.

Based on the Kirchhoff's Voltage Law, the OCV and the voltage derivative of C_1 and C_2 in the second-order RC equivalent circuit model can be described as follows [44]:

$$\begin{cases} \dfrac{\mathrm{d}U_1}{\mathrm{d}t} = -\dfrac{1}{R_1C_1}U_1 + \dfrac{1}{C_1}I \\ \dfrac{\mathrm{d}U_2}{\mathrm{d}t} = -\dfrac{1}{R_2C_2}U_2 + \dfrac{1}{C_2}I \\ U_T = U_{SOC}^{oc} - R_0I - U_1 - U_2 \end{cases} \tag{1}$$

By applying the Laplace transform to Eq (1) for frequency-domain conversion and using the state of charge $SOC(t)$, the electrochemical polarization voltage $U_1(t)$ of the first RC branch, and the concentration polarization voltage $U_2(t)$ of the second RC branch at each moment as the state variable, the continuous-state space equation based on the second-order RC equivalent circuit model for the Lithium-ion battery can be established. It should be noticed that the input current (I) and output terminal voltage (U_T) of the Lithium-ion battery can be obtained through the relevant experimental test.

$$\begin{bmatrix} SOC(t) \\ U_1(t) \\ U_2(t) \end{bmatrix} = \begin{bmatrix} 0 & 0 & 0 \\ 0 & -\frac{1}{R_1C_1} & 0 \\ 0 & 0 & -\frac{1}{R_2C_2} \end{bmatrix} \begin{bmatrix} SOC(t) \\ U_1(t) \\ U_2(t) \end{bmatrix} + \begin{bmatrix} -\frac{1}{Q} & \frac{1}{C_1} & \frac{1}{C_2} \end{bmatrix}^T I(t) + \omega(t) \tag{2}$$

$$U_T(t) = \begin{bmatrix} \dfrac{U_0(SOC(t))}{SOC(t)} & -1 & -1 \end{bmatrix} \begin{bmatrix} SOC(t) \\ U_1(t) \\ U_2(t) \end{bmatrix} - R_0I(t) + v(t) \tag{3}$$

where $w(t)$ and $v(t)$ represent the process noise and measurement noise of the Lithium-ion battery at time t, respectively.

To enable real-time state estimation, Eqs (2) and (3) are discretized to transform them into discrete models, which are very suitable for the processing of the digital controller and the sampled system. The discrete-state space equation for the Lithium-ion battery based on the second-order RC equivalent circuit model can be represented as follows [44]:

$$\begin{bmatrix} SOC(k+1) \\ U_1(k+1) \\ U_2(k+1) \end{bmatrix} = \begin{bmatrix} 1 & 0 & 0 \\ 0 & e^{-\frac{\Delta t}{\tau_1}} & 0 \\ 0 & 0 & e^{-\frac{\Delta t}{\tau_2}} \end{bmatrix} \begin{bmatrix} SOC(k) \\ U_1(k) \\ U_2(k) \end{bmatrix} + \begin{bmatrix} -\frac{\eta \Delta t}{Q} \\ R_1(1-e^{-\frac{\Delta t}{\tau_1}}) \\ R_2(1-e^{-\frac{\Delta t}{\tau_2}}) \end{bmatrix} I(k) + \omega(k) \tag{4}$$

$$U_T(k) = \begin{bmatrix} \frac{\partial U_0(SOC(k))}{\partial SOC(k)} & -1 & -1 \end{bmatrix} \begin{bmatrix} SOC(k) \\ U_1(k) \\ U_2(k) \end{bmatrix} - R_0 I(k) + v(k) \tag{5}$$

where Δt is the sampling period, η denotes the discharge efficiency, and $w(k)$ and $v(k)$ represent the process noise and the observation noise, respectively, $\tau_1 = R_1 C_1$, and $\tau_2 = R_2 C_2$, respectively.

3. Preliminary parameter identification

Based on the above-mentioned second-order RC equivalent circuit model for the Lithium-ion battery, we identify the corresponding parameters and estimate the battery SOC. To obtain the operating voltage and current data, a battery test platform is established, as shown in Figure 2. It comprises a host computer, a middle-level machine based on a digital controller, a NEWARE battery tester, and a programmable temperature control box. During the testing process, the charge or discharge profile is loaded by the NEWARE battery tester. Through the voltage and current sampling and signal conversion, the middle-level machine collects and store the voltage/current data and then transfer the data to the host computer. The programmable temperature control box ensures a constant operating temperature or a specific operating temperature for the lithium-ion battery. In addition, battery fixtures are individually designed using 3D printing technology to guarantee the reliability and security during the clamping test. The round cell fixture includes an insulating base printed based on nylon material and positive and negative L-shaped components made of aluminum, and is covered with insulating baked paint.

In this study, the Wubin-18650 lithium-ion battery is utilized for the experimental testing. Owing to its excellent low-temperature performance and high discharge rate, this Wubin-18650 lithium-ion battery can effectively match the low-temperature and high-power application scenarios of EVs and other energy storage or power supply systems. The rated capacity of this Wubin-18650 lithium-ion battery is 2376 mAh. The OCV, UDDS, HPPC, and DST test conditions are conducted at room temperature (i.e., 25 °C).

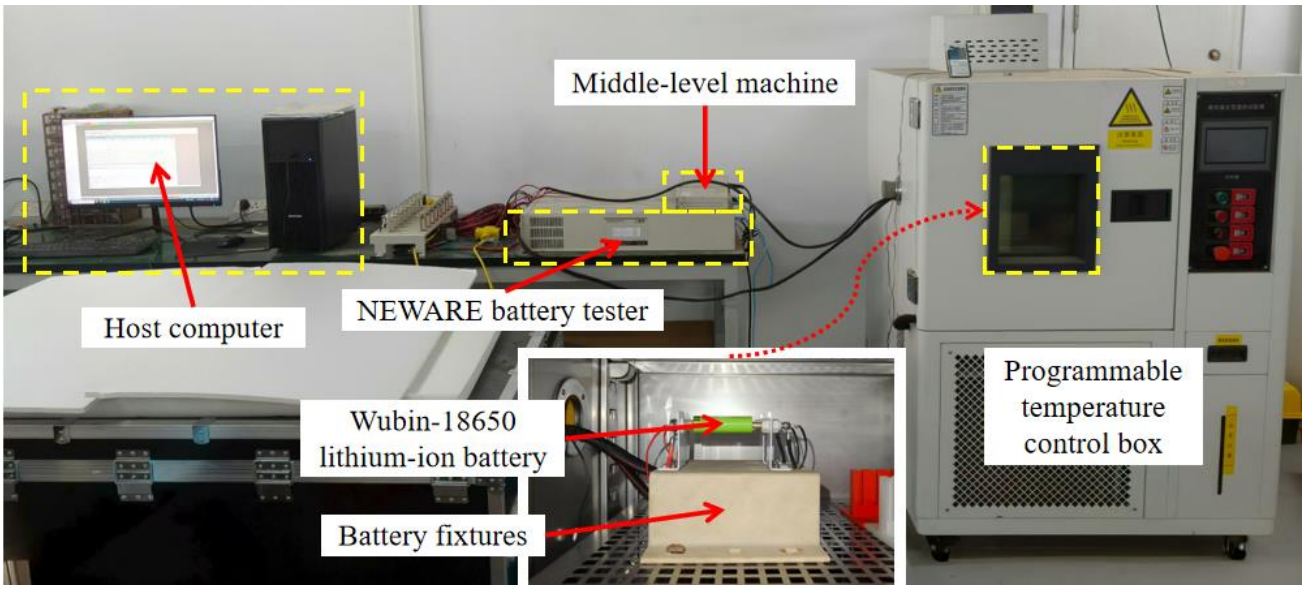

Figure 2. Test platform for the lithium-ion battery.

Based on the experimental test, the voltage-current characteristic curves under the four test conditions are shown in Figure 3. On this basis, the OCV of the Lithium-ion battery can be expressed as a specific functional relationship in accordance with its SOC [45]. To support the subsequent parameter identification and the corresponding SOC estimation, a ninth-order polynomial fitting function is utilized to reflect the relationship between the OCV and the corresponding SOC of the lithium-ion battery, as depicted in Eq (6). The fitting results is illustrated in Figure 4(a).

$$\begin{aligned} U_{SOC}^{OC} &= b_0 SOC^9 + b_1 SOC^8 + b_2 SOC^7 + b_3 SOC^6 + b_4 \cdot SOC^5 \\ &+ b_5 SOC^4 + b_6 SOC^3 + b_7 SOC^2 + b_8 SOC + b_9 \end{aligned} \tag{6}$$

where b_i denotes the fitting coefficients of the function, in which $i = 0, 1\ldots, 9$.

With the OCV test, the terminal voltage variation of the lithium-ion battery is illustrated in Figure 4(b). During the C-E interval, the pulse discharge current is turned to zero, which corresponds to a zero-input response for the two RC networks. In this case, the D-E interval can be fitted using the following equation [46]:

$$U_T(t) = U_{SOC}^{oc} - U_1(t_c)e^{\frac{-(t-t_c)}{\tau_1}} - U_2(t_c)e^{\frac{-(t-t_c)}{\tau_2}} \tag{7}$$

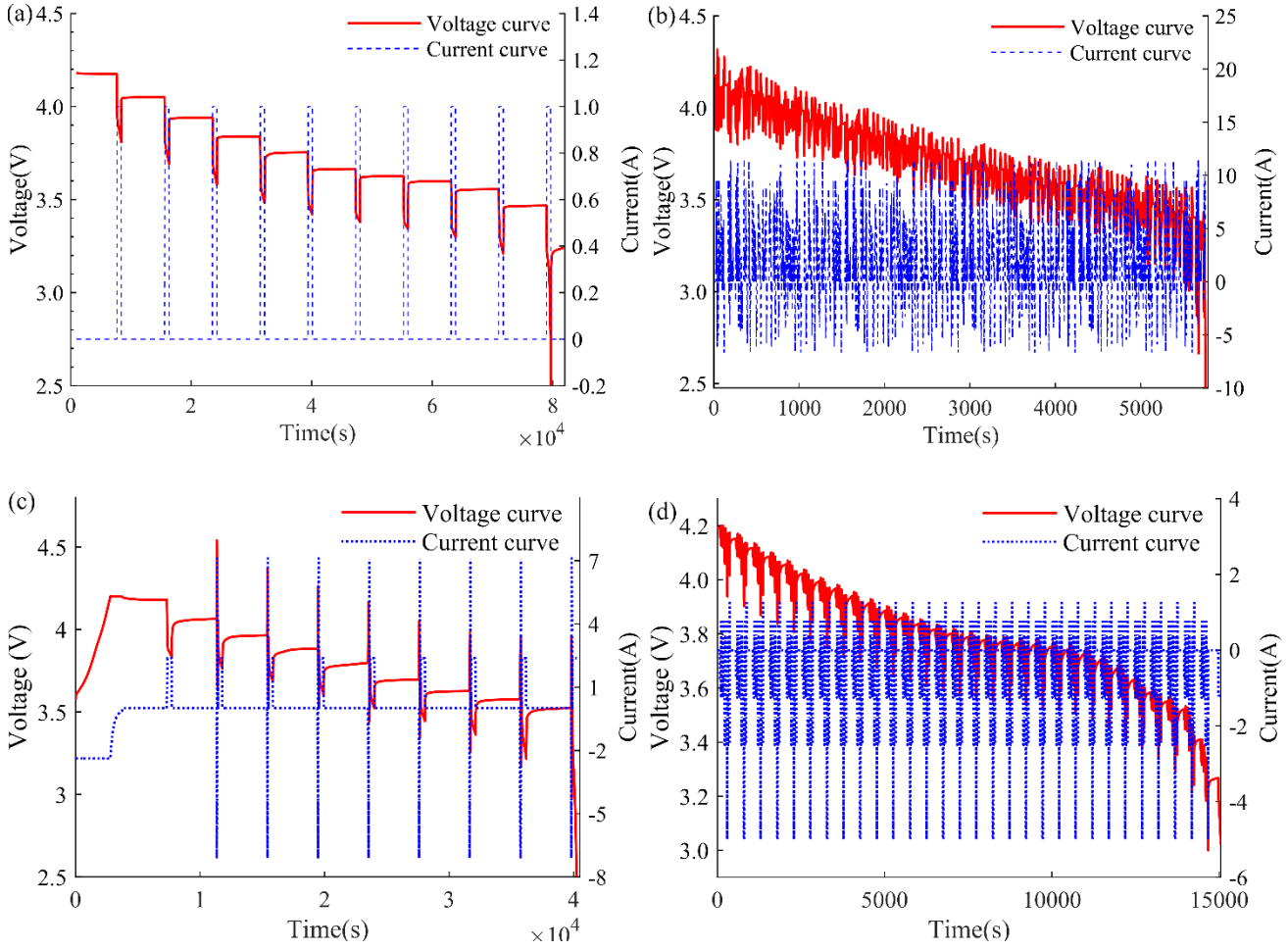

Figure 3. Voltage-current characteristic curves. (a) Under the OCV test condition, (b) Under the UDDS test condition, (c) Under the HPPC test condition, and (d) Under the DST condition.

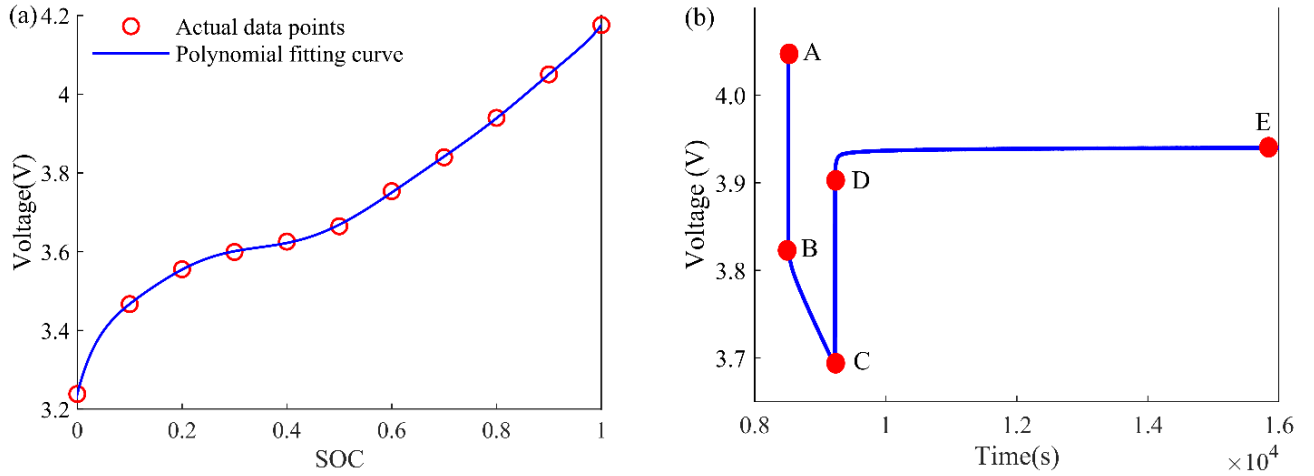

Figure 4. OCV characteristic and terminal voltage characteristic. (a) Curve fitting based on the OCV-SOC characteristic and (b) Terminal voltage characteristic during a selected period (from 8500 s to 16000 s) of the OCV test shown in Figure 3(a).

The model parameters of the second-order RC equivalent circuit model for the Lithium-ion battery at each SOC can be calculated as follows [44]:

$$\begin{cases} R_0 = \dfrac{|U(t_B) - U(t_A)| + |U(t_D) - U(t_C)|}{2|i_L|} \\ R_i = \dfrac{U_i(t_c)}{i_L} \\ C_i = \dfrac{\tau_i}{R_i} \end{cases} \tag{8}$$

As shown in Figure 4(b), the instantaneous voltage drops near the start of the pulse (around point B) and the voltage recovery at the end are used to calculate parameters such as R_0 for the battery model based on Eq (8). Furthermore, by repeating this analysis at each SOC level, a complete set of initial battery parameters varying with SOC is obtained. This set of offline identified parameters provides reliable initial values for the subsequent TRLS optimization, which effectively mitigate the risk of the algorithm converging to a local optimum due to poor initial values. The final optimized parameters obtained via the TRLS algorithm are presented and discussed in detail in Section 4.

To enhance the identification accuracy, an offline identification method based on the LM algorithm is first implemented [47]. The LM algorithm combines the advantages of the gradient descent method and the Gauss-Newton method. As an optimization algorithm for solving nonlinear least squares problems, it can achieve highly efficient and good convergence by dynamically adjusting the damping factor.

$$r(\varphi) = \left[U_T(t_1) - \hat{U}_T(t_1, \varphi) \quad \cdots \quad U_T(t_n) - \hat{U}_T(t_n, \varphi) \right]^{\mathrm{T}} \tag{9}$$

where $U_T(t_i)$ represents the observed value and $\hat{U}_T(t_i, \varphi)$ denotes the predicted value of the model with the parameter φ, in which φ is the parameter vector that needs to be optimized. Here, $\varphi = [U_1(t_c), 1/\tau_1, U_2(t_c), 1/\tau_2]^{\mathrm{T}}$, where $U_1(t_c)$, $1/\tau_1$, $U_2(t_c)$ and $1/\tau_2$ are the parameters to be determined.

By using the residual sum of squares as the objective function, a suitable parameter φ to achieve the minimum value of $S(\varphi)$ is found.

$$S(\varphi) = r(\varphi)^{\mathrm{T}} r(\varphi) = \sum_{i=1}^{n} \left[U_T(t_i) - \hat{U}_T(t_i, \varphi) \right]^2 \tag{10}$$

Subsequently, the parameter update is achieved by constructing the Jacobian matrix of the residual vector $r(\varphi)$ with respect to parameter vector φ.

$$(J_k^{\mathrm{T}} J_k + \lambda_k I) \Delta\varphi = -J_k^{\mathrm{T}} r(\varphi_k) \tag{11}$$

where J_k and λ_k represent the Jacobian matrix and the damping factor at the current iterative step, respectively, I denotes the identity matrix, $\Delta\varphi$ represents the parameter update, and the parameter is updated as: $\varphi_{k+1} = \varphi_k + \Delta\varphi$.

Furthermore, the damping factor λ_k should be dynamically adjusted to ensure the control

performance. If the objective function is $S(\varphi_{k+1}) < S(\varphi_k)$, the damping factor is appropriately reduced. Otherwise, it would be increased. If the change in the objective function $S(\varphi)$ falls below a preset threshold or the norm of the parameter update $\Delta\varphi$ is less than a preset threshold, the iteration would be stopped. In this case, the optimal fitting parameters can be determined. Subsequently, the preliminary identification results of the physical parameters R_0, R_1, R_2, C_1, and C_2 are obtained by substituting the optimized vector $\varphi = [U_1(t_c), 1/\tau_1, U_2(t_c), 1/\tau_2]^{\mathrm{T}}$ into Eq (8).

4. TRLS-based optimization for parameter identification

For the above parameter identification of second-order RC equivalent circuit model, the offline identification is employed to obtain initial parameter values, which can be subsequently used for the online identification [48,49]. This hybrid identification strategy significantly improves the convergence speed and the estimation accuracy. Furthermore, by optimizing the offline identification parameters, the overall robustness and computational efficiency for the parameter estimation is improved, while the sensitivity or uncertainty to the unsuitable initial parameters for the SOC estimation is effectively reduced.

The TRLS-based optimization algorithm is an efficient nonlinear optimization method that integrates the gradient information with a quadratic approximation model [50]. It can adaptively adjust the trust-region radius based on the difference between the actual value and the predicted value, thereby ensuring global convergence, numerical stability, and high accuracy. At each iteration, the TRLS-based optimization algorithm dynamically constrains the update step for the identification of the physical parameters $\theta = [R_0, R_1, R_2, C_1, C_2]^{\mathrm{T}}$ within the trust region, thereby preserving the validity of the quadratic model approximation. It should be noticed that, as a nonlinear optimization method, the TRLS algorithm is sensitive to initial values. By preprocessing the battery model parameters and using the LM algorithm, we can provide initial guesses close to the true values, thereby preventing the TRLS from converging to local optima.

In the parameter optimization process, the physical parameters θ are set to be identified at different SOC points. We select an SOC interval of 0.1, a choice based on the trade-off between estimation accuracy and computational complexity [51,52]. Specifically, an overly sparse interval may fail to adequately capture the nonlinear variations of parameters under dynamic operating conditions, thereby introducing significant errors, whereas an overly dense interval would substantially increase the computational burden of parameter identification and significantly raise the storage requirements of the BMS. Considering the critical importance of real-time performance and resource consumption in practical BMS applications, we adopt an SOC interval of 0.1, aiming to ensure parameter identification accuracy while balancing computational efficiency and resource optimization.

By defining the sum of squared residuals as the objective function $S(\theta)$, the proposed TRLS-based method approximates the objective function $S(\theta)$ with a second-order model within the trust region.

$$m_k(\Delta\theta) = S(\theta_k) + \frac{1}{2}\Delta\theta^{\mathrm{T}} H_k \Delta\theta + Y_k^{\mathrm{T}}\Delta\theta \tag{12}$$

where Y_k and H_k represent the Jacobian matrix and the Hessian matrix of the objective function $S(\theta)$, respectively, and $\Delta\theta$ denotes the parameter update variation, i.e., the search step size.

Figure 5 depicts the detailed iterative procedure based on the Steihaug-Toint truncated conjugate gradient (Steihaug–CG) method.

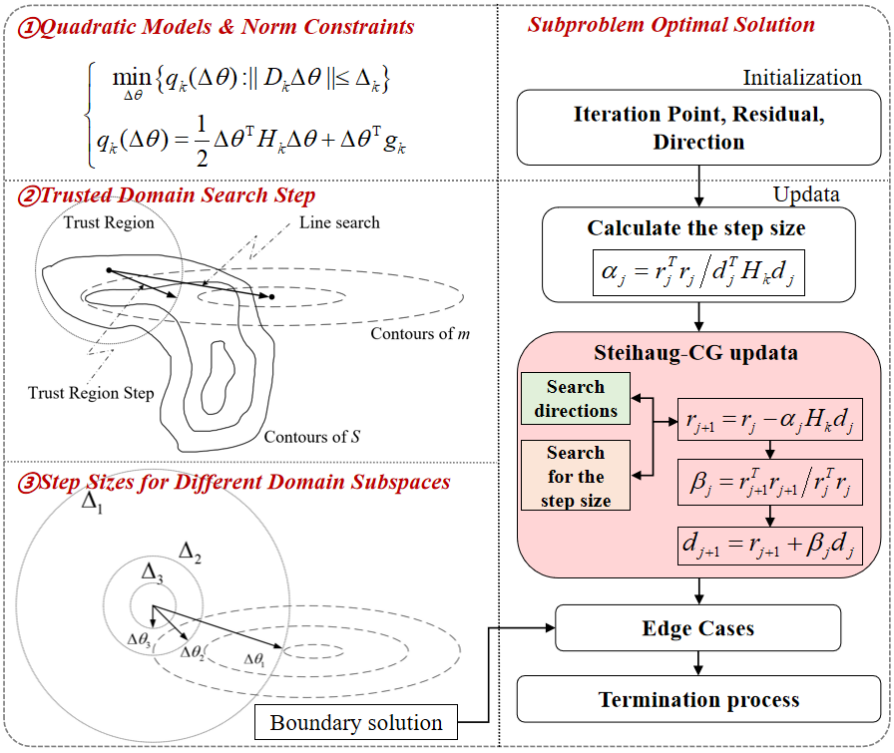

Figure 5. Flowchart for the solution of the trust-region subproblem.

In Figure 5, the efficient solution of the trust-region subproblem is central to the TRLS-based optimization algorithm [50], as shown in Eq (13).

$$\begin{cases} \min\limits_{\Delta\theta}\{q_k(\Delta\theta):\| D_k\Delta\theta \|\leq \Delta_k\} \\ q_k(\Delta\theta)=\frac{1}{2}\Delta\theta^{\mathrm{T}}H_k\Delta\theta+\Delta\theta^{\mathrm{T}}g_k \end{cases} \tag{13}$$

where q_k, D_k, and Δ_k denote the gradient vector of the objective function, the diagonal scaling matrix, and the trust-region radius at the k_{th} iteration, respectively.

With the quadratic model and radius constraint, the algorithm dynamically explores along conjugate-gradient directions. Whenever the curvature remains positive definite and the step lies inside the trust region, the standard conjugate gradient (Standard CG) method updates continuously. However, if the curvature is negative or the step exceeds the radius, the current direction must be immediately retracted to the boundary. This strategy delivers an approximate minimizer that satisfies the norm restriction and ensures sufficient descent condition, which is achieved with the matrix-vector product rather than the explicit Hessian factorization.

If the candidate step $\Delta\theta$ yields the sufficient descent condition in the objective function, it can be accepted as the new iteration, and the trust-region radius can be either retained or enlarged to accelerate convergence. Otherwise, the radius should be contracted and a revised step would be computed by resolving the trust-region subproblem. The iterative process of the TRLS-based

optimization algorithm is illustrated in Figure 6. The algorithm's core mechanism lies in its dynamic adjustment of the trust region radius Δ_k during each iteration k, based on the consistency between the actual reduction in the objective function S and the predicted reduction from model q_k, quantified by ratio ρ_k. When ρ_k exceeds a predefined threshold, the step $\Delta\theta$ is accepted, parameters are updated to $\theta_{k+1} = \theta_k + \Delta\theta$, and Δ_k is doubled to accelerate convergence. For moderate ρ_k values, the step is accepted with Δ_k maintained to enhance robustness. Conversely, when ρ_k falls below the threshold, indicating poor model approximation, the parameters remain unchanged, and Δ_k is halved to prevent divergence. This iterative process continues until convergence criteria are satisfied.

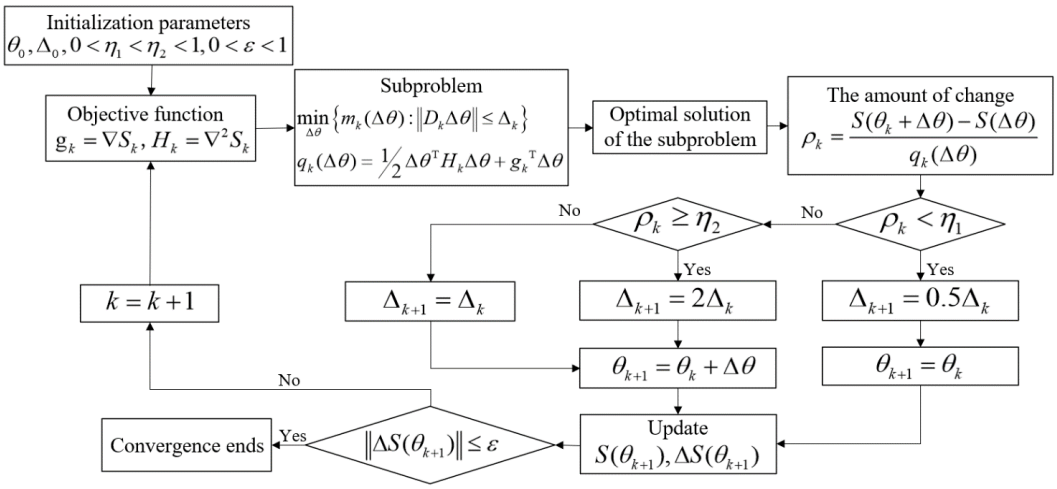

Figure 6. The iterative process of the TRLS optimization algorithm.

With the TRLS-based optimization algorithm, the parameter identification model for the second-order RC equivalent circuit model of the Lithium-ion battery is constructed based on the MATLAB/Simulink. The experimental current and voltage data are imported into this Simulink model. The parameters are then optimized through the above-mentioned TRLS-based optimization algorithm. Moreover, the relationships among the five major parameters of the second-order RC equivalent circuit model and the battery SOC are obtained, as shown in Table 1.

Table 1. Identified parameters of the second-order RC equivalent model.

SOC	0.1	0.2	0.3	0.4	0.5	0.6	0.7	0.8	0.9	1.0
R_0/mΩ	19.8	20.3	21.8	20.2	19.6	19.4	19.2	19.5	20.2	21.3
R_1/mΩ	0.49	0.51	0.51	0.51	0.49	0.51	0.50	0.50	0.50	0.50
R_2/mΩ	0.5040	0.495	0.502	0.496	0.497	0.503	0.497	0.501	0.505	0.499
C_1/kF	20.59	19.70	19.68	19.21	20.30	19.71	19.93	19.87	20.09	19.92
C_2/kF	197.1	203.1	198.9	203.5	204.5	200.4	202.1	200.7	197	199.3

To systematically validate the effectiveness of the TRLS-based parameter identification and optimization algorithm, we construct a detailed simulation model and conducted a comparative analysis between the model's predicted values and high-precision actual measurement results. In evaluating the prediction accuracy, the Mean Absolute Error (MAE) and Standard Deviation (SD) are selected as key performance indicators, with their calculation formulas provided in Eqs (14) and (15),

respectively [47]. The MAE intuitively reflects the average deviation level of the voltage predictions, while the SD is used to measure the dispersion and stability of the predicted values. Together, these metrics provide a comprehensive assessment of the algorithm's overall performance. In the validation strategy, the OCV test serves primarily as a static benchmark condition to verify the static accuracy and consistency of the model parameters under quasi-equilibrium states, rather than evaluating dynamic estimation performance. The validation of dynamic performance relies on three standard driving cycles, namely UDDS, HPPC, and DST test conditions. These dynamic test conditions effectively stimulate the complete dynamic response of the battery model, providing a reliable basis for assessing the accuracy of the parameter identification in practical applications.

$$\mathrm{MAE} = \frac{1}{n}\sum_{i=1}^{n}\left|z_i - \hat{z}_i\right| \tag{14}$$

$$\mathrm{SD} = \sqrt{\frac{1}{n}\sum_{i=1}^{n}\left(\hat{z}_i - \bar{z}\right)^2} \tag{15}$$

where z_i, $\hat{z}_i$, and $\bar{z}$ represent the true value, the prediction value, and the mean value, respectively.

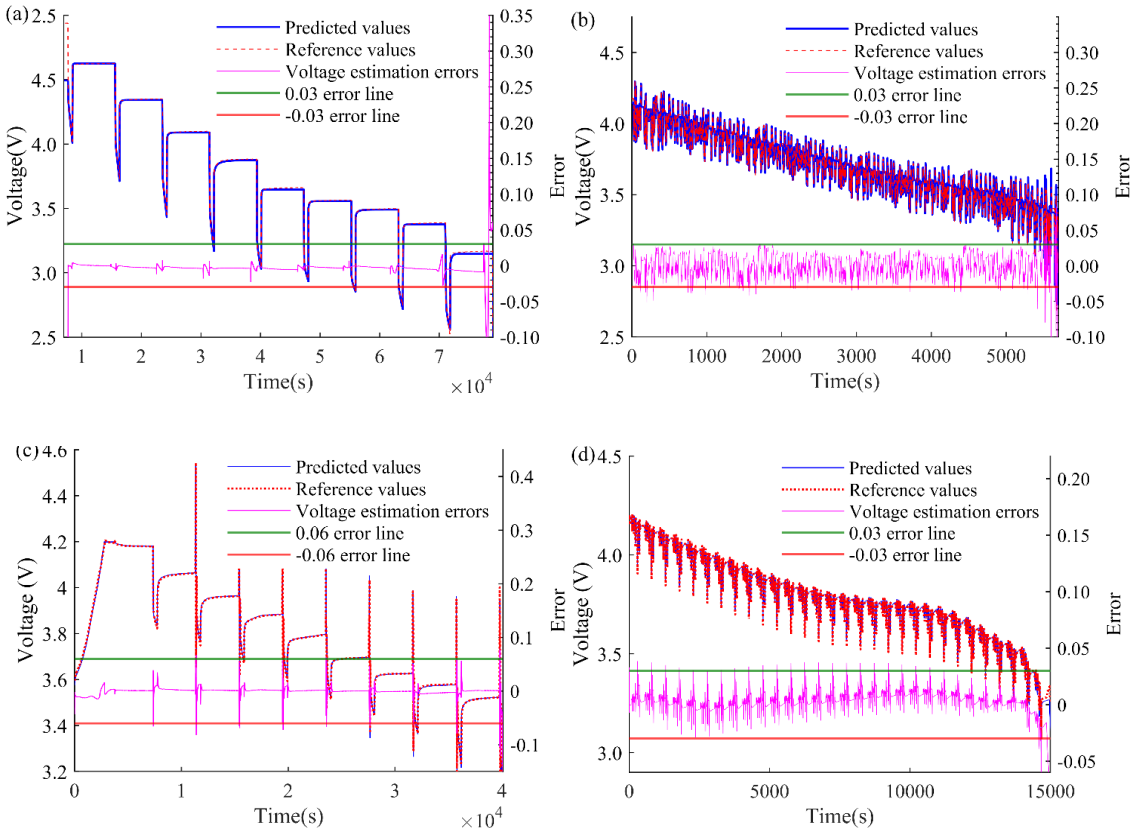

Figure 7. Terminal voltage estimation under the four test conditions. (a) Terminal voltage estimation under the OCV test condition, (b) Terminal voltage estimation under the UDDS test condition, (c) Terminal voltage estimation under the HPPC test condition, and (d) Terminal voltage estimation under the DST condition.

The comparative results shown in Figure 7 demonstrate a high degree of consistency between the simulated and measured voltages under the static OCV test condition and three dynamic test conditions (i.e., UDDS, HPPC, and DST). The MAEs of the fitted terminal voltages for the four conditions are 0.0099 V, 0.012 V, 0.0045 V, and 0.0073 V, respectively, while the corresponding SDs are 0.029, 0.015, 0.020, and 0.014, respectively. These results successfully prove that the second-order RC equivalent circuit model, with parameters optimized by the TRLS algorithm, can accurately reproduce the dynamic voltage characteristics of lithium-ion batteries under various operating conditions. This achievement lays a solid foundation for accurate battery state estimation.

5. SOC Estimation

As one of core parameters of the battery management system, the SOC directly reflects the remaining charge of the battery [53,54]. It is also a key indicator for optimizing the power distribution among battery cells, extending the battery life, and ensuring stable operation of the overall lithium-ion battery system. With the constant temperature and the discharge/charge rate, the battery SOC can be defined as follows:

$$SOC(t) = \frac{Q_{rem}(t)}{Q} \times 100\% \tag{16}$$

where $Q_{rem}(t)$ and Q represent the real-time capacity and the rated capacity of the lithium-ion battery, respectively.

Accurate SOC estimation can prevent over-charge and over-discharge while enhancing the overall battery system performance [55,56]. Among model-based approaches for the battery SOC estimation, the EKF has been widely adopted for nonlinear estimation because of its mature theoretical foundation, straightforward implementation, and noise-suppression capability.

In a classical EKF algorithm, as described in Eq (17), the current state x_k is initially predicted using the estimated state x_{k-1} based on the previous step and the current system input u_k. Then, the current state estimation error covariance P_k is predicted by combining the process noise covariance matrix Q_k. Furthermore, the Kalman gain K_k is adjusted through Eq (18) to balance the influence of the observed values on the state estimation. Finally, Eq (19) is applied to update the system state and the state estimation error covariance by incorporating the observed values and the Kalman gain, which enables the recursive estimation. As shown in Figure 8, it shows the detailed iterative steps of the EKF algorithm. However, under dynamic conditions, time-varying parameters of the battery model introduce significant nonlinearities that degrade the tracking accuracy of the EKF. To address the limitation of the EKF, in the following, a DEKF algorithm is developed. The DEKF algorithm uses two independent Kalman filters to concurrently estimate state variables and model parameters, thereby enhancing the adaptive ability to the parameter variation and improving the robustness under complex operating conditions.

$$\begin{cases} x_k^- = f(x_{k-1}^+, u_{k-1}) \\ P_k^- = A_{k-1} P_{k-1}^+ A_{k-1}^{\mathrm{T}} + Q_{k-1} \end{cases} \tag{17}$$

$$K_k = (P_k^- C_k^{\mathrm{T}})(C_k P_k^- C_k^{\mathrm{T}} + R_k)^{-1} \tag{18}$$

$$\begin{cases} x_k^{+} = x_k^{-} + K_k\left[y_k - g(x_k^{-}, u_k)\right] \\ P_k^{+} = (I - K_k C_k) P_k^{-} \end{cases} \tag{19}$$

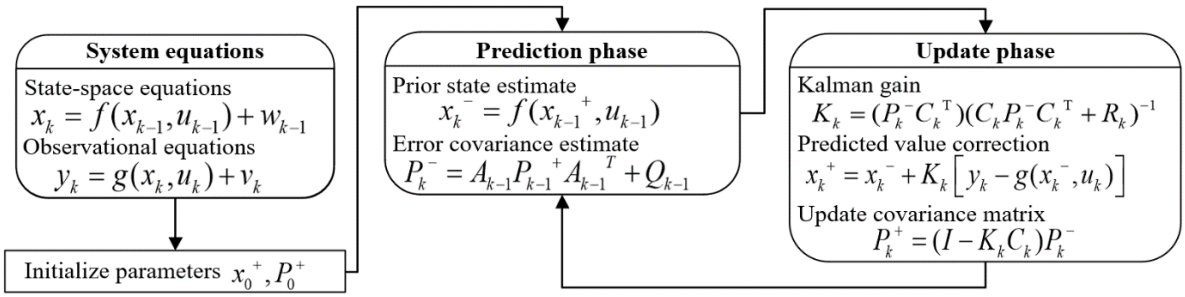

Figure 8. Flowchart for the EKF algorithm.

Based on the optimization framework derived from the TRLS algorithm, the DEKF method is implemented to achieve high-accuracy SOC estimation. The procedure, illustrated in Figure 9, begins with the initialization of system variables. This includes the initial state vector, which comprises SOC and polarization voltages, along with the initial error covariance matrix. Furthermore, this initialization establishes the foundation for the subsequent recursive estimation process.

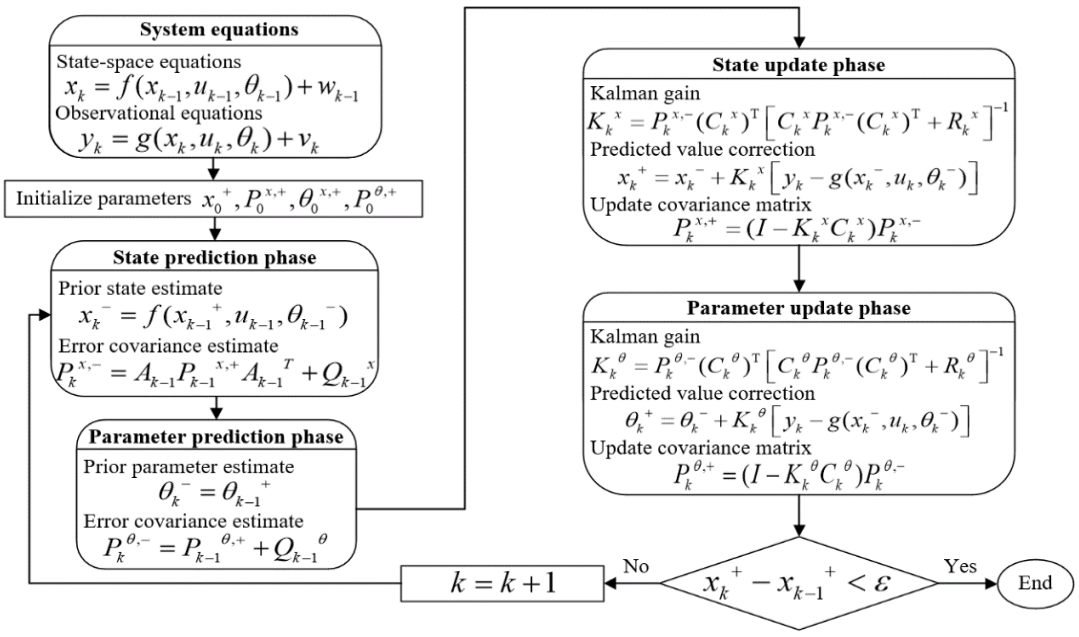

Figure 9. Flowchart for the DEKF method.

The DEKF operates through a dual-iteration mechanism, systematically executing prediction and updating steps in the state and parameter filters. In the state filter, the state-space model incorporates parameters identified via TRLS to predict the system state. Specifically, the state transition function propagates the prior state forward in time, while the observation function maps the updated state to the predicted terminal voltage. Furthermore, the parameter filter refines the model parameters in real time

to adapt to dynamic operational conditions, ensuring ongoing model accuracy.

As depicted in Figure 9, the DEKF minimizes estimation variance by recursively integrating the prior state estimate, updated parameters, and real-time current and voltage measurements. At each sampling interval, the Kalman gain is computed to optimally weight the new observations, thereby correcting both the state and parameter estimates. This iterative process ensures robust and precise SOC tracking under varying load profiles, effectively balancing model-based predictions with measurement-based corrections. The integration of TRLS-optimized parameters significantly enhances the model's fidelity, contributing to improved convergence behavior and estimation stability throughout diverse discharge and charge cycles.

Within this framework, the nonlinear second-order RC equivalent circuit model can be represented as follows [57]:

$$\begin{cases} x_k = Ax_{k-1} + Bu_{k-1} + w_{k-1} \\ y_k = Cx_k + Du_k + v_k \end{cases} \tag{20}$$

where x_k, y_k, and u_k represent the state variable, measurement vector, and system input of the system, respectively, A and B denote the system state transition matrix and input matrix, respectively, and C and D represent the system output matrix and feedthrough matrix, respectively.

The state and measurement equations can be linearized according to Eq (21).

$$\begin{cases} x_k \approx f(\hat{x}_{k-1}, u_{k-1}) + \dfrac{\partial f}{\partial \hat{x}_{k-1}}(x_{k-1} - \hat{x}_{k-1}) + w_{k-1} \\ y_k \approx g(\hat{x}_k, u_{k-1}) + \dfrac{\partial g}{\partial \hat{x}_k}(x_k - \hat{x}_k^-) + v_k \end{cases} \tag{21}$$

To verify the effectiveness of the DEKF algorithm under different operating conditions, the simulation and experiment comparisons are conducted under the static OCV test condition and the three dynamic test conditions (i.e., UDDS, HPPC, and DST), respectively. It should be noticed that the SOC estimation method combines the TRLS-based optimization solution of model parameters with the DEKF algorithm, which is defined as the proposed TRLS-based method. Moreover, the SOC estimation method combined the TRLS-based optimization solution of model parameters with the conventional EKF algorithm is defined as the conventional EKF-based method. Based on the definition, the estimation results of the battery SOC using the conventional EKF-based method and the proposed TRLS-based method under the four test conditions are shown in Figure 10(a)–(d), respectively.

The comparative results are shown in Tables 2–5. With the conventional EKF-based method, the MAEs of the SOC estimation under the OCV, UDDS, HPPC, and DST test conditions are 0.0071, 0.019, 0.011, and 0.0095, respectively, while the corresponding SDs of the SOC estimation errors are 0.0047, 0.011, 0.0069, and 0.0094, respectively. As a comparison, with the proposed TRLS-based method, the MAEs for the SOC estimation under the four test conditions are 0.0031, 0.0066, 0.0052, and 0.0044, respectively, while the corresponding SDs of the SOC estimation errors are 0.0014, 0.0041, 0.0035, and 0.0039, respectively.

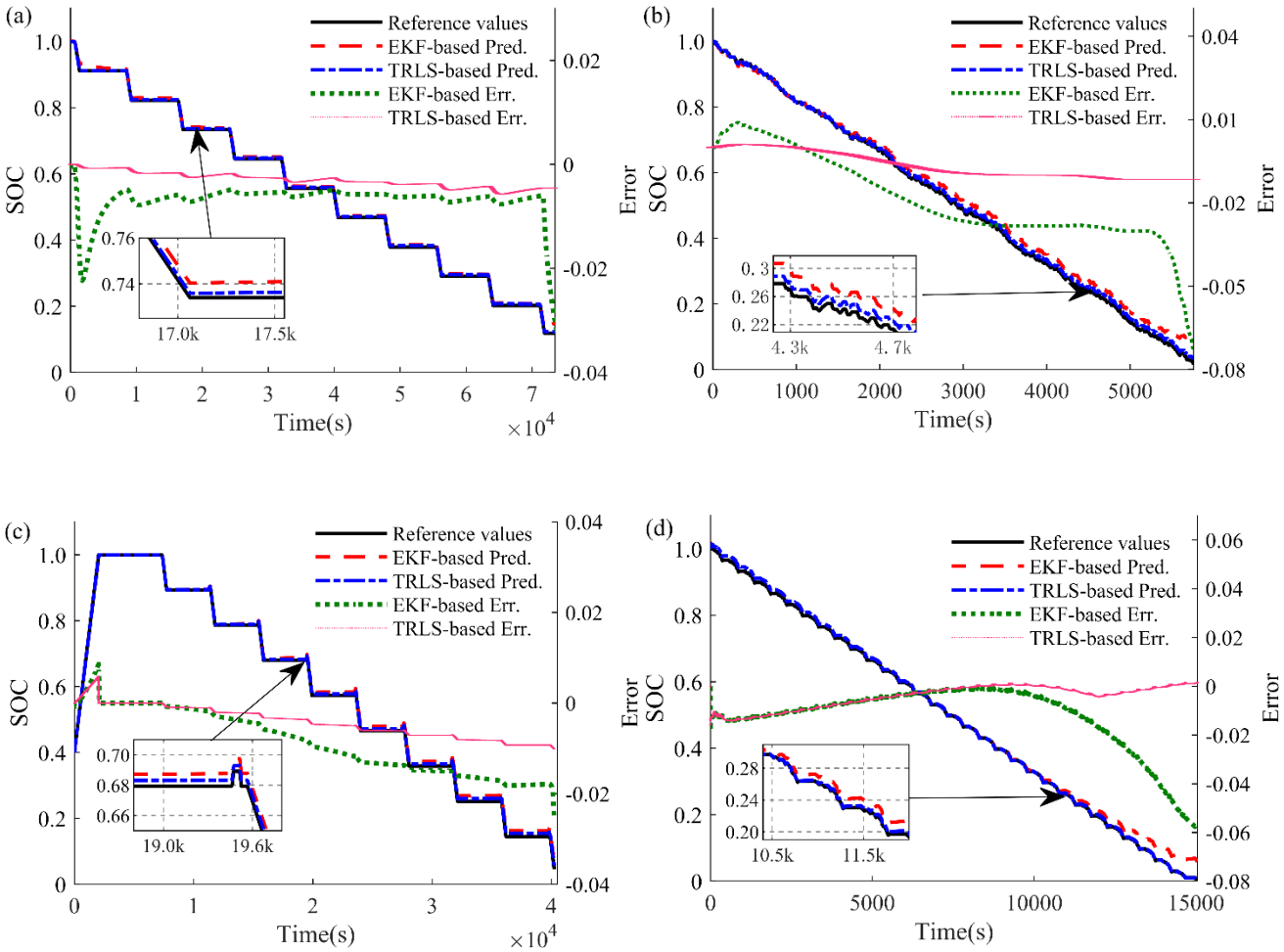

Figure 10. SOC estimation results. (a) SOC estimation under the OCV test condition, (b) SOC estimation under the UDDS test condition, (c) SOC estimation under the HPPC test condition, and (d) SOC estimation under the DST condition.

Notes: The abbreviations in the legend are defined as follows: "EKF-based Pred." and "TRLS-based Pred." stand for the predicted values of the EKF-based and TRLS-based methods, respectively; and "EKF-based Err." and "TRLS-based Err." represent the estimation errors of the corresponding methods.

Table 2. Comparison of the absolute SOC estimation errors under the static OCV test condition.

SOC	0.1	0.2	0.3	0.4	0.5	0.6	0.7	0.8	0.9
EKF-based method	0.0197	0.0072	0.0062	0.0060	0.0051	0.0054	0.0048	0.0059	0.0048
TRLS-based method	0.0046	0.0054	0.0037	0.0035	0.0027	0.0026	0.0017	0.0016	0.0017

Table 3. Comparison of the absolute SOC estimation errors under the UDDS test condition.

SOC	0.1	0.2	0.3	0.4	0.5	0.6	0.7	0.8	0.9
EKF-based method	0.0300	0.0290	0.0280	0.0280	0.0260	0.0190	0.0100	0.0010	0.0057
TRLS-based method	0.0110	0.0100	0.0090	0.0093	0.0091	0.0065	0.0033	0.0005	0.0008

Table 4. Comparison of the absolute SOC estimation errors under the HPPC test condition.

SOC	0.1	0.2	0.3	0.4	0.5	0.6	0.7	0.8	0.9
EKF-based method	0.0188	0.0178	0.0154	0.0145	0.0126	0.0089	0.0052	0.0026	0.0005
TRLS-based method	0.0096	0.0087	0.0076	0.0065	0.0054	0.0042	0.0029	0.0017	0.0005

Table 5. Comparison of the absolute SOC estimation errors under the DST condition.

SOC	0.1	0.2	0.3	0.4	0.5	0.6	0.7	0.8	0.9
EKF-based method	0.0310	0.0155	0.0050	0.0012	0.0010	0.0037	0.0062	0.0093	0.0124
TRLS-based method	0.0014	0.004	0.0020	0.0006	0.0008	0.0035	0.0060	0.0095	0.0115

To intuitively display the advantage of the proposed TRLS-based method for the SOC estimation, a 3D bar chart is used to compare and analyze the comprehensive estimation effect of the two estimation methods under the two test conditions, as shown in Figure 11. With the unique dual-filter structure of the DEKF algorithm, the proposed TRLS-based method decouples the state estimation from parameter estimation, thereby avoiding the error propagation caused by the coupling of state estimation and parameter estimation in the conventional EKF-based method. Compared with the conventional EKF-based algorithm, the proposed TRLS-based method more accurately estimates the SOC of the lithium-ion battery through the collaborative estimation of states and model parameters. Additionally, by updating estimated parameters in real time, it better adapts to the dynamic change characteristics of the battery, which significantly reduces the estimation error during the initial and final stages of discharge. The comparative result successfully validates the rationality and validity of the proposed TRLS-based method.

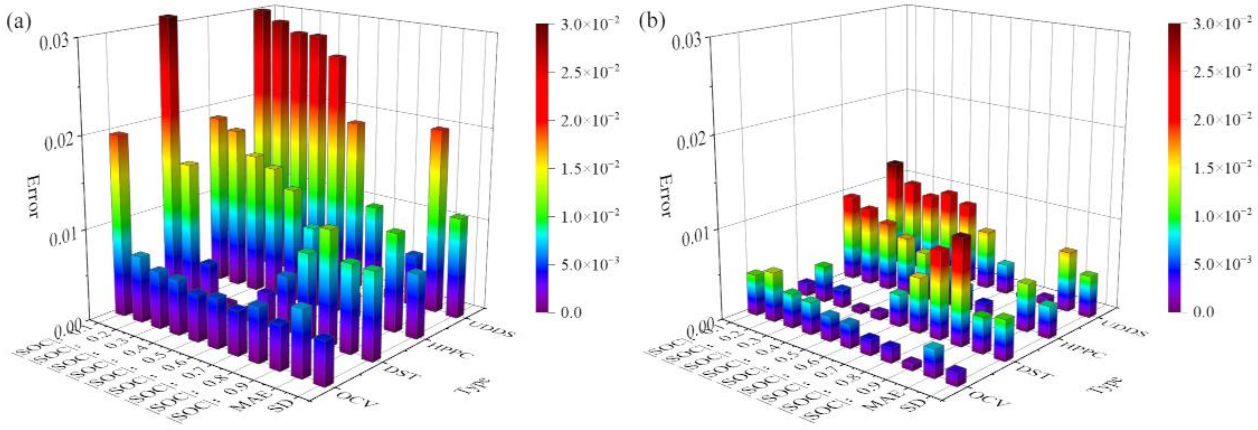

Figure 11. 3D bar chart for the SOC estimation errors of the two methods. (a) The EKF-based method and (b) the TRLS-based method.

6. Conclusions

In this study, we successfully developed a TRLS-based method for the parameter identification and SOC estimation of lithium-ion batteries. Initially, a second-order RC equivalent circuit model was established to reflect the dynamic operation performance of lithium-ion batteries. A battery testing

platform was constructed, and the Wubin lithium-ion battery was selected for discharge experiments under four test conditions. The model parameters of the second-order RC equivalent circuit were preliminarily identified using the LM algorithm, followed by parameter optimization using the TRLS algorithm. Ultimately, the optimized parameters from TRLS were integrated with the DEKF method to achieve SOC estimation. The innovation of this study lies in the hybrid strategy based on the TRLS and the DEKF, which is suitable for the nonlinear dynamic optimization and parameter identification of lithium-ion batteries. Specifically, the TRLS algorithm significantly enhances the initial parameter identification accuracy by constructing a local approximation model within the trust region during the offline phase. This provides a more stable and accurate initial point for the DEKF method, mitigating the effects of initial value bias and nonlinearity. Moreover, the DEKF can decouple state and parameter estimation using its dual-filter structure. The parameter filter in the DEKF method adjusts only the observable subspace during online operation, ensuring long-term adaptability through online fine-tuning. By combining the TRLS-based parameter identification method with the DEKF method for battery SOC estimation, the proposed TRLS-based method can effectively improve computational accuracy and reliability.

The comparative analyses between the simulation and experimental results were conducted to verify the effectiveness of the proposed TRLS-based method. Our results showed that under the OCV, UDDS, HPPC, and DST test conditions, the MAEs between the simulated voltage and the measured voltage were 0.0099 V, 0.0118 V, 0.0045 V, and 0.0073 V, respectively. Additionally, when the proposed TRLS-based method was used for battery SOC estimation, the MAEs under the four test conditions were 0.0031, 0.0066, 0.0052, and 0.0044, respectively. Compared to the conventional EKF-based method, the proposed TRLS-based method exhibited superior performance in terms of accuracy, robustness, and applicability.

Looking ahead, the proposed TRLS-based battery SOC estimation method shows significant potential for enhancing the real-time performance and reliability of BMSs in future energy systems, particularly in the electric vehicle applications. In addition, in future work, we will focus on the artificial intelligence optimization for the proposed TRLS-based method. In particular, a temperature-adaptive TRLS algorithm based on artificial intelligence optimization will be developed to ensure the accuracy of SOC estimation under dynamic temperature operating conditions. In this way, the method will be extended to large-scale battery systems, such as grid-level energy storage, to ensure its effectiveness in high-capacity applications.

Use of AI tools declaration

The authors declare they have not used Artificial Intelligence (AI) tools in the creation of this article.

Acknowledgments

This research was funded by the Aeronautical Science Foundation of China (Grant No. 2024Z039070003) and the Key Research and Development Program of Shaanxi Province (Grant No. 2023-YBGY-376).

Conflict of interest

The authors declare no conflicts of interest.

Author contributions

Jun Wang: Software, Writing—original draft, Formal analysis. Dexing Wang: Conceptualization, Methodology, Writing—review & editing. Hui Li: Software, Writing—review & editing. Chao Ma: Data curation, Visualization, Validation, Writing—review & editing. Changhai Liu: Data curation, Validation, Writing—review & editing. Bin Wang: Resources, Supervision, Writing—review & editing, Funding acquisition.

References

1. He M, Hector LJ, Dai F, et al. (2024) Industry needs for practical lithium-metal battery designs in electric vehicles. *Nat Energy* 9: 1199–1205. https://doi.org/10.1038/s41560-024-01624-5
2. Miao K, Ma C, Zhou J (2025) Advances and prospects of low temperature Li-S batteries. *Appl Energy* 388: 125720. https://doi.org/10.1016/j.apenergy.2025.125720
3. Andersson M, Streb M, Prathimala V, et al. (2024) Electrochemical model-based aging-adaptive fast charging of automotive lithium-ion cells. *Appl Energy* 372: 123644. https://doi.org/10.1016/j.apenergy.2024.123644
4. Geslin A, Xu L, Ganapathi D, et al. (2025) Dynamic cycling enhances battery lifetime. *Nat Energy* 10: 172–180. https://doi.org/10.1038/s41560-024-01675-8
5. Kurucan M, Özbaltan M, Yetgin Z, et al. (2024) Applications of artificial neural network based battery management systems: A literature review. *Renewable Sustainable Energy Rev* 192: 114262. https://doi.org/10.1016/j.rser.2023.114262
6. Wu L, Lyu Z, Huang Z, et al. (2024) Physics-based battery SOC estimation methods: Recent advances and future perspectives. *J Energy Chem* 89: 27–40. https://doi.org/10.1016/j.jechem.2023.09.045
7. Degen F, Winter M, Bendig D, et al. (2023) Energy consumption of current and future production of lithium-ion and post lithium-ion battery cells. *Nat Energy* 8: 1284–1295. https://doi.org/10.1038/s41560-023-01355-z
8. Kong C, Zhu G, Wang J, et al. (2025) A simplified electrochemical lithium-ion batteries model based on-informed LSTM_Res network. *Int J Heat Mass Transfer*, 246. https://doi.org/10.1016/j.ijheatmasstransfer.2025.127024
9. Fornaro P, Puleston P, Battaiotto P (2023) State-of-Charge and State-of-Health variable-gain estimation based on tracking sliding mode differentiators for an electric vehicle Lithium-ion battery. *J Energy Storage*, 65. https://doi.org/10.1016/j.est.2023.107298
10. Li J, Bai G, Yan J, et al. (2024) On-line parameter identification and SOC estimation of nonlinear model of lithium-ion battery based on Wiener structure. *J Energy Storage*, 92. https://doi.org/10.1016/j.est.2024.112094
11. Miranda D, Gonçalves R, Wuttke S, et al. (2023) Overview on theoretical simulations of lithium-ion batteries and their application to battery separators. *Adv Energy Mater*, 13: 2203874. https://doi.org/10.1002/aenm.202203874

12. Tang A, Huang Y, Xu Y, et al. (2024) Data-physics-driven estimation of battery state of charge and capacity. *Energy*, 294. https://doi.org/10.1016/j.energy.2024.130776
13. Chen M, Xie X, He C, et al. (2025) An integrated framework for ARX model identification and its application to lithium-ion battery. *IEEE Trans Instrum Meas* 74: 1-14. https://doi.org/10.1109/TIM.2025.3545698
14. Wang J, Du J, Tan B, et al. (2023) Establishment of a lithium-ion battery model considering environmental temperature for battery state of charge estimation. *J Electrochem Soc* 170: 120507. https://doi.org/10.1149/1945-7111/ad11af
15. Li H, Fu L, Long X, et al. (2024) A hybrid deep learning model for lithium-ion batteries state of charge estimation based on quantile regression and attention. *Energy*, 294. https://doi.org/10.1016/j.energy.2024.130834
16. Wang S, Wu Y, Zhou H, et al. (2025) Improved particle swarm optimization-adaptive dual extended Kalman filtering for accurate battery state of charge and state of energy joint estimation with efficient core factor feedback correction. *Energy* 322: 135686. https://doi.org/10.1016/j.energy.2025.135686
17. Jiang Z, Zhang Y, Gao R (2025) An improved electrochemical-thermal coupling model for state-of-charge estimation of lithium-ion battery. *Energy* 333: 137486. https://doi.org/10.1016/j.energy.2025.137486
18. Li Z, Zhang X, Gao W (2024) State of health estimation of lithium-ion battery during fast charging process based on BiLSTM-Transformer. *Energy* 311: 133418. https://doi.org/10.1016/j.energy.2024.133418
19. Li F, Zuo W, Zhou K, et al. (2024) State-of-charge estimation of lithium-ion battery based on second order resistor-capacitance circuit-PSO-TCN model. *Energy* 289: 130025. https://doi.org/10.1016/j.energy.2023.130025
20. Yuan B, Zhang B, Yuan X, et al. (2024) Study on the estimation of the state of charge of lithium-ion battery. *Electrochim Acta* 491: 144297. https://doi.org/10.1016/j.electacta.2024.144297
21. Li N, Zhang X, Wang R, et al. (2025) SR-CKF algorithm-based state-of-charge estimation of lithium-ion batteries for energy storage over a wide temperature range. *J Energy Storage*, 125: 116849. https://doi.org/10.1016/j.est.2025.116849
22. Wang D, Yang Y, Gu T (2023) A hierarchical adaptive extended Kalman filter algorithm for lithium-ion battery state of charge estimation. *J Energy Storage* 62: 106831. https://doi.org/10.1016/j.est.2023.106831
23. Ding F (2023) Least squares parameter estimation and multi-innovation least squares methods for linear fitting problems from noisy data. *J Comput Appl Math* 426: 115107. https://doi.org/10.1016/j.cam.2023.115107
24. Huang C (2023) An online condition-based parameter identification switching algorithm for lithium-ion batteries in electric vehicles. *IEEE Trans Veh Technol* 72: 1701–1709. https://doi.org/10.1109/TVT.2022.3210688
25. Hou J, Liu J, Chen F, et al. (2023) Robust lithium-ion state-of-charge and battery parameters joint estimation based on an enhanced adaptive unscented Kalman filter. *Energy* 271: 126998. https://doi.org/10.1016/j.energy.2023.126998
26. Wang J, Song J, Li Y, et al. (2024) State of charge estimation for lithium-ion battery based on improved online parameters identification and adaptive square root unscented Kalman filter. *J Energy Storage* 77: 109977. https://doi.org/10.1016/j.est.2023.109977

27. Yang J, Fang W, Chen J, et al. (2022) A lithium-ion battery remaining useful life prediction method based on unscented particle filter and optimal combination strategy. *J Energy Storage* 55: 105648. https://doi.org/10.1016/j.est.2022.105648
28. Jiang Z, Qin S, Wei Y, et al. (2021) An immune genetic extended kalman particle filter approach on state of charge estimation for lithium-ion battery. *Energy* 230: 120805. https://doi.org/10.1016/j.energy.2021.120805
29. Ananda S, Lakshminarasamma N, Radhakrishna, et al. (2022) Lithium-ion cell sorting and cell performance modeling for spacecraft battery. *IEEE Trans Ind Appl* 58: 6536–6545. https://doi.org/10.1109/TIA.2022.3179455
30. Li N, He F, Ma W, et al. (2022) An indirect state-of-health estimation method based on improved genetic and back propagation for online lithium-ion battery used in electric vehicles. *IEEE Trans Veh Technol* 71: 12682–12690. https://doi.org/10.1109/TVT.2022.3196225
31. Zhang F, Xing Z, Wu M (2023) State of health estimation for Li-ion battery using characteristic voltage intervals and genetic algorithm optimized back propagation neural network. *J Energy Storage* 57: 106277. https://doi.org/10.1016/j.est.2022.106277
32. Liu Y, Zhao W, Yin G (2024) Forgetting-Factor regrets for online convex optimization. *IEEE Trans Autom Control* 69: 5034–5048. https://doi.org/10.1109/TAC.2023.3340120
33. Cao R, Zhang Z, Shi R, et al. (2025) Model-constrained deep learning for online fault diagnosis in Li-ion batteries over stochastic conditions. *Nat Commun* 16: 1651. https://doi.org/10.1038/s41467-025-56832-8
34. Liu Z, He H, Xie J, et al. (2022) Self-discharge prediction method for lithium-ion batteries based on improved support vector machine. *J Energy Storage* 55: 105571. https://doi.org/10.1016/j.est.2022.105571
35. Ren X, Liu S, Yu X, et al. (2021) A method for state-of-charge estimation of lithium-ion batteries based on PSO-LSTM. *Energy* 234: 121236. https://doi.org/10.1016/j.energy.2021.121236
36. Sharma S, Garg A, Panigrahi B (2024) Predicting state-of-charge using gradient-boosted SVR ensemble technique for lithium ion battery used in EVs. *IEEE Trans Transp Electrification* 10: 4441–4454. https://doi.org/10.1109/TTE.2023.3310159
37. Shi J, Rivera A, Wu D (2022) Battery health management using physics-informed machine learning: Online degradation modeling and remaining useful life prediction. *Mech Syst Signal Process* 179: 109347. https://doi.org/10.1016/j.ymssp.2022.109347
38. Liu M, Zhou X, Yang L, et al. (2023) A novel Kalman-filter-based battery internal temperature estimation method based on an enhanced electro-thermal coupling model. *J Energy Storage* 71: 108241. https://doi.org/10.1016/j.est.2023.108241
39. Wang C, Yang M, Wang X, et al. (2025) A review of battery SOC estimation based on equivalent circuit models. *J Energy Storage* 110: 115346. https://doi.org/10.1016/j.est.2025.115346
40. Su S, Li W, Mou J, et al. (2023) A hybrid battery equivalent circuit model, deep learning, and transfer learning for battery state monitoring. *IEEE Trans Transp Electrification* 9: 1113–1127. https://doi.org/10.1109/TTE.2022.3204843
41. Zhu G, Hu M, Qiu C, et al. (2025) Integer variable-order equivalent circuit model and switching strategy for lithium-ion power batteries for vehicles based on information criterion under dynamic and static working conditions. *Energy* 322: 135694. https://doi.org/10.1016/j.energy.2025.135694

42. Hong Z, Wang Y, Jin Z (2025) Diagnosis of battery external short circuits based on an improved second-order RC fault model and recursive least squares identification method. *Energy* 319: 134880. https://doi.org/10.1016/j.energy.2025.134880
43. Xiong R, Pan Y, Shen W, et al. (2020) Lithium-ion battery aging mechanisms and diagnosis method for automotive applications: Recent advances and perspectives. *Renewable Sustainable Energy Rev* 131: 110048. https://doi.org/10.1016/j.rser.2020.110048
44. Monirul I, Qiu L, Ruby R (2024) Accurate SOC estimation of ternary lithium-ion batteries by HPPC test-based extended Kalman filter. *J Energy Storage* 92: 112304. https://doi.org/10.1016/j.est.2024.112304
45. Yan Y, Wang B, Wang C, et al. (2024) Adaptive maximum available energy evaluation for lithium battery in hydrogen-electric hybrid unmanned aerial vehicle applications considering dynamic ambient temperature and aging level. *Energy Convers Manage* 314: 118685. https://doi.org/10.1016/j.enconman.2024.118685
46. Wei L, Lin T, Wang Y (2025) CCEM: Cell-to-Cell Extension Model for low-cost joint estimation of SOC and temperature in supercapacitor series modules. *J Energy Storage* 119: 116316. https://doi.org/10.1016/j.est.2025.116316
47. Paul T, Wang S, Zhang H, et al. (2023) An ASTSEKF optimizer with nonlinear condition adaptability for accurate SOC estimation of lithium-ion batteries. *J Energy Storage* 70: 108098. https://doi.org/10.1016/j.est.2023.108098
48. Fan Y, Zhang Z, Yang G, et al. (2025) A comparative study of modeling and parameter identification for lithium-ion batteries in energy storage systems. *Measurement* 243: 116263. https://doi.org/10.1016/j.measurement.2024.116263
49. Yang B, Wang D, Sun X, et al. (2023) Offline order recognition for state estimation of Lithium-ion battery using fractional order model. *Appl Energy* 341: 120977. https://doi.org/10.1016/j.apenergy.2023.120977
50. Duan Z, Hong X, Li H, et al. (2024) Simulating the uneven temperature distributions within large-sized lithium-ion batteries using a thermal resistance network model. *J Energy Storage* 101: 113732. https://doi.org/10.1016/j.est.2024.113732
51. Peng J, Meng J, Wu J, et al. (2023) A comprehensive overview and comparison of parameter benchmark methods for lithium-ion battery application. *J Energy Storage* 71: 108197. https://doi.org/10.1016/j.est.2023.108197
52. Wang Y, Cheng Y, Xiong Y, et al. (2022) Estimation of battery open-circuit voltage and state of charge based on dynamic matrix control-extended Kalman filter algorithm. *J Energy Storage* 52: 104860. https://doi.org/10.1016/j.est.2022.104860
53. Wu J, Lei D, Liu Z, et al. (2024) A fusion algorithm of multidimensional element space mapping architecture for SOC estimation of lithium-ion batteries under dynamic operating conditions. *Energy* 311: 133467. https://doi.org/10.1016/j.energy.2024.133467
54. Zhou Z, Duan B, Li C, et al. (2025) Life-cycle state-of-charge estimation for lithium-ion battery considering coulomb efficiency and capacity decay. *IEEE Trans Transp Electrification* 11: 6335–6343. https://doi.org/10.1109/TTE.2024.3506778
55. Tang A, Huang Y, Liu S, et al. (2023) A novel lithium-ion battery state of charge estimation method based on the fusion of neural network and equivalent circuit models. *Appl Energy* 348: 121578. https://doi.org/10.1016/j.apenergy.2023.121578

56. Xu M, Zhang E, Wang S, et al. (2024) Dynamic ultrasonic response modeling and accurate state of charge estimation for lithium ion batteries under various load profiles and temperatures. *Appl Energy* 355: 122210. https://doi.org/10.1016/j.apenergy.2023.122210
57. Zhang Y, Lai X, Zhang X, et al. (2025) Fusion of stress and electrical signals for high-accuracy joint estimation of SOC and SOH in lithium-ion batteries. *Energy* 331: 137063. https://doi.org/10.1016/j.energy.2025.137063